Dalton Transactions

ROYAL SOCIETY OF CHEMISTRY

PAPER

View Article Online
View Journal | View Issue

Cite this: *Dalton Trans.*, 2023, **52**, 11698

Turn-on fluorescence of ruthenium pyrene complexes in response to bovine serum albumin†

Saša Opačak, Margareta Pernar Kovač, Anamaria Brozovic, Ivo Piantanida* and Srećko I. Kirin *

Received 19th July 2023,
Accepted 25th July 2023

DOI: 10.1039/d3dt02289g

rsc.li/dalton

Two novel pyrene triphenylphosphine ruthenium conjugates act as fluorescent turn-on beacons for serum albumin, being non-fluorescent in aqueous media but exhibiting strong emission upon binding to BSA. The selective cytotoxicity of the compounds against tumour cells is enhanced upon irradiation by UV-light, paving the way for application in photodynamic therapy under two-photon excitation.

Introduction

The detection of bovine serum albumin (BSA) is of interest in many fields of research as it is often used as a model protein for human serum albumin, which plays an important role in metabolism. Fluorescence is an attractive method for sensor applications as it is fast, practical, highly sensitive and selective. Multiple fluorescent BSA probes are described in the literature, with sensors that exhibit "light-up" aggregation-induced emission (AIE) being especially prominent.[1–4] They are desired in a variety of applications, such as bioimaging, biosensors, and photodynamic therapy. Over the past few decades, photodynamic therapy (PDT), as a photo-regulated treatment modality for cancers and other diseases, has received widespread attention.[5] It involves the incorporation of disease-site accumulated photosensitizers, light and oxygen to generate toxic reactive oxygen species (ROS) to kill cancer cells and destroy disease tissues.[6]

The covalently linked pyrene functional group is especially interesting due to its unique sensing properties, such as intense blue emission, high fluorescence quantum yield, long-lived singlet excited state, and long emission lifetime (>100 ns), as well as its pronounced hydrophobicity. Many pyrene derivatives show intriguing biorelevant interactions, and, as strong chromophores and fluorophores, act as probes for bio-macromolecules such as various DNA/RNA sequences.[7–19] Pyrene can form non-covalent interactions with DNA/RNA such as aromatic stacking intercalation into DNA/RNA, binding within the DNA minor groove *via* a combination of hydrophobic and edge-to-face aromatic interactions, or by forming a pyrene excimer within the DNA minor groove or RNA major groove. Pyrene is also prone to form an exciplex in combination with other chromophores.[20,21] Due to these properties, pyrene is a sensitive fluorescent probe widely used for characterization of different micro-heterogeneous systems.[22–28]

In spite of their potential carcinogenic properties, substituted pyrenes and their organometallic complexes may serve as anti-cancer agents.[29–31] Photodynamic therapy is another avenue for the application of pyrene compounds although their non-favourable excitation wavelength (350–400 nm) is far too short for efficient PDT due to low tissue permeability at these wavelengths, as wavelengths of >600 nm would be required.[32] Recent developments in two-photon-absorption (TPA) allow the application of doubled excitation wavelengths for efficient excitation of photosensitisers[33,34] and enable the use of pyrenes for biomedical applications.[35,36] Ruthenium complexes have been widely studied as potential anticancer drugs with several compounds, reaching phase II of clinical trials.[37] Triphenylphosphine Ru complexes have previously been explored as anticancer compounds.[38–41] Amino acid analogues of the compounds in this paper have shown micromolar toxicity and relevant binding affinity for proteins.[42] Previously, we employed compounds with similar structures in catalytic enantioselective hydrogenation[43] and as a chiroptical switch.[44]

So far, only a few small molecules have shown fluorescence light-up sensing of serum albumins.[45] Hua *et al.*[46] reported on a sensor based on diketopyrrolopyrrole with ammonium groups, which is nearly non-emissive in aqueous solution but shows strong emission in the near-infrared region upon binding with BSA. A couple of other sensors based on Ru-complexes or pyrene analogues have shown enhancement of their intrinsic fluorescence upon BSA binding.[47–49]

In this paper, we designed and prepared two novel ruthenium-pyrene conjugates **1** and **2** (Fig. 1) by linking triphenylphosphine and pyrene with a flexible linker and then complexing one or two ligands with Ru(*p*-cymene)Cl_2. Therefore, the

Ruđer Bošković Institute, Bijenička cesta 54, HR-10000 Zagreb, Croatia.
E-mail: Srecko.Kirin@irb.hr, Ivo.Piantanida@irb.hr

† Electronic supplementary information (ESI) available. See DOI: https://doi.org/10.1039/d3dt02289g

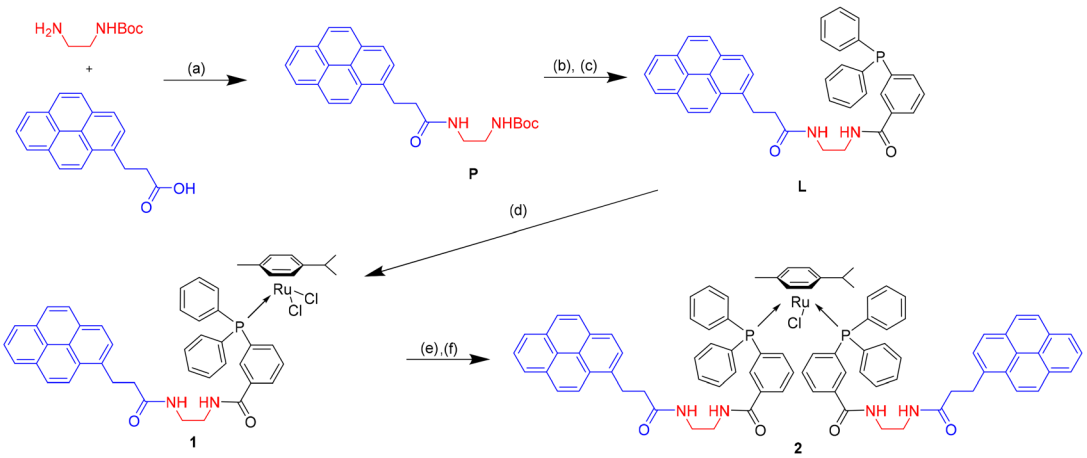

Fig. 1 Synthesis of complexes **1** and **2**, precursor **P** and ligand **L**. (a) TBTU, HOBt, DCM, 24–48 h, room temperature; (b) TFA/DCM 1/1, 2 h, room temperature; (c) 3-(diphenylphosphino)benzoic acid, TBTU, HOBt, DCM, 24–48 h, room temperature; (d) ligand **L**, di-μ-chlorobis[(*p*-cymene)clororuthenium(II)], DCM, 2 h, room temperature; (e) mono-complex **1**, NH_4PF_6, ACN, reflux 45 min, evaporation; and (f) solid residue from (e), **L**, DKM, 24 h, room temperature.

designed mono-pyrene analogue **1** is expected to intramolecularly fold due to the strongly hydrophobic nature of pyrene and eventually form an interaction between the Ru-cation (and/or triphenylphosphine) and pyrene, whereas bis-derivative **2** has an alternative way of forming an intramolecular pyrene exciplex. The intramolecularly folded structure of **1** or **2** rearranges upon binding to a biorelevant target (protein), due to the requirements of the binding site, and consequently strongly changes its spectrophotometric properties. Moreover, since both the Ru-cation and pyrene are known for photo-induced bioactivity, irradiation upon binding to a biorelevant target is expected to result in strong cytotoxicity. Thus, novel compounds are designed to act as theranostic probes, with combined fluorometric sensing and photoactivated bioactivity.

Results and discussion

Synthesis

Synthesis was performed in solution in several steps (Fig. 1). In the first step, 1-pyrenebutyric acid was coupled to Boc-ethylenediamine *via* TBTU/HOBt coupling reagents and DIPEA as the base affording precursor **P**. In the next step, the BOC protecting group was removed by stirring **P** in a 1/1 solution of TFA/DCM for two hours and the resulting unprotected amine was reacted with *m*-triphenylphosphino-benzoic acid using the TBTU/HOBt (DIPEA) coupling protocol, yielding ligand **L**.

The mono-ruthenium complex was synthesised by mixing ligand **L** and the metal precursor $[Ru(p\text{-cymene})Cl_2]_2$ in DCM and stirring the mixture overnight at room temperature. The mono-Ru complex **1** was then purified by column chromatography (5% MeOH in DCM). The bis-ruthenium complex **2** was synthesised by dissolving the mono-Ru complex **1** and NH_4PF_6 in acetonitrile and stirring the solution at reflux for 45 minutes. The solution was then evaporated, and the residue dissolved in DCM along with an additional ligand **L** and stirred at room temperature for 24 hours. The complex **2** was purified by column chromatography (1–2% MeOH in DCM). Ligand **L** and complexes **1** and **2** were characterised by ^{1}H, ^{13}C and ^{31}P NMR spectroscopy, HRMS and spectrophotometric methods. The characteristic shifts in the ^{31}P NMR spectra of complexes **1** (δ_p = 23.08 ppm) and **2** (δ_p = 20.97 ppm) clearly indicate the binding of **L** to the Ru-cation, in comparison with the free ligand **L** (δ_p = −5.27 ppm).[42]

Spectroscopic characterisation

Compounds **1** and **2** are poorly soluble in water. In order to study them under biorelevant conditions, stock solutions in DMSO (1 mM) were freshly prepared for each experiment and diluted in buffer (sodium cacodylate buffer, I = 50 mM, pH 7.0) prior to measurement. The measured spectra were also compared to those of the referent compound 1-pyrenebutyric acid. We have focused our discussion on compound **2**.

The absorbance of the aqueous solutions of **1** and **2** was proportional to their concentrations up to $c = 1 \times 10^{-5}$ M (Fig. S2–S5†). However, a systematic increase of the baseline (>400 nm) at c(**1**, **2**) > 3×10^{-6} M indicates the formation of a colloid (Fig. S2–S5†), likely caused by the aggregation of strongly hydrophobic compounds. Heating the solution to 90 °C caused irreversible precipitation. Thus, the absorption maxima and their corresponding molar extinction coefficients, given in ESI Table S1,† were derived from the concentrations prior to aggregation. Colloid formation was not observed for DMSO solutions, pointing out that aggregation is specific to aqueous solutions. The UV/Vis spectra of all studied compounds collected in DMSO are identical to the referent 1-pyrenebutyric acid (Fig. 2b), in contrast to the UV/Vis spectra in an aqueous buffer, where **L**, **1** and **2** show a significant bathochromic shift in comparison with the referent 1-pyrenebutyric acid

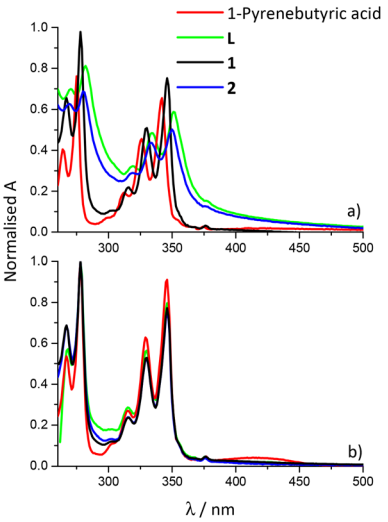

Fig. 2 Comparison of UV/vis spectra of 1-pyrenebutyric acid,[59] **L**, **1** and **2** at concentration $c = 2 \times 10^{-6}$ M in: (a) water, and (b) DMSO.

(Fig. 2a), indicating that the pyrene chromophore is most likely engaged in aromatic stacking interactions.

Both **1** and **2**, dissolved in DMSO, exhibit characteristic pyrene fluorescence (Fig. S7 and S9†), which is completely quenched in aqueous media (Fig. S10†), while ligand **L** exhibits a pyrene exciplex peak at 500 nm,[50] and the referent 1-pyrenebutyric acid shows a well-resolved set of emission maxima in the 380–400 nm range, which is typical of free pyrene emission (Fig. 3). Intriguingly, heating the aqueous solution of **2** to 90 °C and cooling it back to 25 °C resulted in the appearance of a weak emission spectrum closely resembling the emission of the referent 1-pyrenebutyric acid (Fig. 3). The observed results suggest a significant impact of the Ru-cation on the emission properties of pyrene. Ligand **L**, having no metal cation, seems to fold into an intramolecular pyrene–triphosphine exciplex, as previously noted for pyrene–quinoline[51] or pyrene–phenanthridine[52] conjugates. The possibility of intermolecular pyrene–pyrene excimer formation was excluded due to the emission proportionality to the concentration of **L**. However, the complexation of **L** with the Ru-cation, yielding **1** or **2**, resulted in complete loss of pyrene emission, strongly

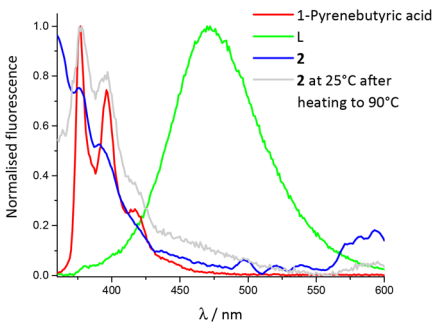

Fig. 3 Normalised fluorescence spectra of **L**, 1-pyrenebutyric acid, **2** and **2** after heating to 90 °C and subsequent cooling to 25 °C.

supporting an intramolecular non-radiative decay mechanism involving a metal cation, which again could be partially diminished by heating the solution of the complex. These results indicate that the complexes in aqueous solutions are, due to their lipophilic nature, in a compact folded conformation, which enables the interaction of pyrenes with the metal cation.

The excitation spectra of all the compounds closely resemble their UV/vis spectra, indicating that the same chromophore is responsible for absorption and emission (Fig. S8†). It seems that the non-covalent intramolecular interaction of pyrene with the Ru-cation is responsible for the total quenching of pyrene emission in complex **1** or **2**. Consequently, any interaction with another target, which would impact the intramolecular self-folding in **1** or **2**, restores the pyrene emission to some extent. Since the pyrene compounds that we have studied earlier have shown biorelevant interactions with both *ds*DNA and proteins (SA),[19,20,51] we studied the interactions of **1** and **2** with model DNA (*ct*DNA) and protein (BSA) herein.

The addition of *ct*DNA did not influence the non-emissive properties of **1** and **2**, and the thermal denaturation points (Fig. S6, S15 and S16†) or chiral properties (Fig. S19 and S20†) of *ct*DNA. The ethidium bromide displacement assays[53] revealed IDA_{50} (indicator displacement assay) values of 0.016 and 0.050 (Fig. S17 and S18†). Thus, complexes **1** and **2** do not interact significantly with *ds*DNA.

However, the addition of BSA resulted in the appearance of strong emission of **1** and **2** (Fig. 4), closely resembling the emission of free pyrene in 1-pyrenebutyric acid and differing significantly from the excimer emission of ligand **L**. This would imply that pyrene(s) of **1** or **2** are, upon binding into the BSA binding site, detached from the intramolecular interaction with the Ru-cation and did not engage in any other aromatic interaction.

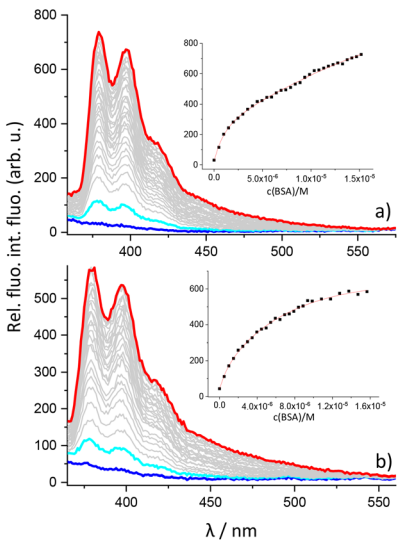

Fig. 4 Titration of (a) **1** and (b) **2** ($c = 5 \times 10^{-6}$ M; λ_{exc} = 340 nm) with BSA; inset graphs show the dependence of fluorescence at λ_{max} = 380 nm on *c*(BSA); non-linear fit to 1 : 1 stoichiometry (—).

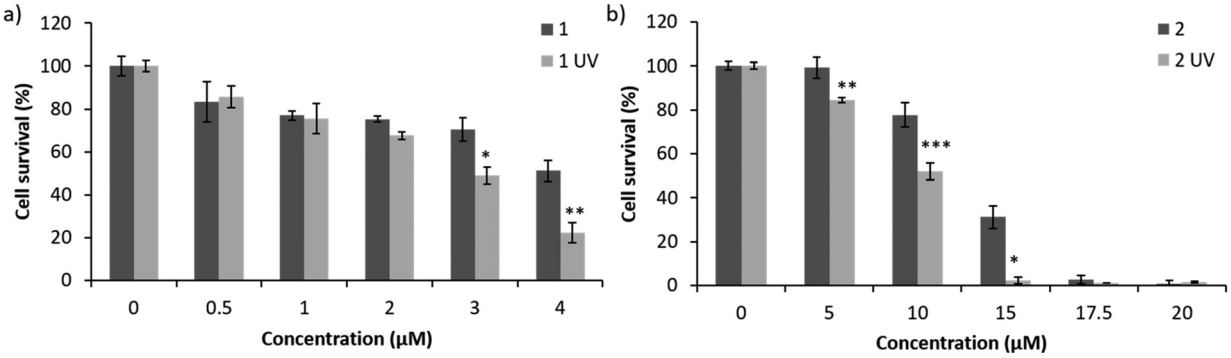

Fig. 5 Viability of HeLa cells treated with **1** (a) or **2** (b) with and without 350 nm irradiation. All data are expressed as the average percentage of the viability values relative to an untreated or only irradiated control ± SD. Significance was determined between the treated and irradiated cells compared with the treated cells only using the paired *t* test (**P* < 0.05; ***P* < 0.01; ****P* < 0.001).

For more detailed characterisation, we determined fluorescence decays by time-correlated single photon counting (TC-SPC) for complexes **1**/BSA and **2**/BSA, which were bi-exponential (**1**/BSA: 15.3 and 123.7 ns; **2**/BSA: 22.1 and 130.8 ns) and significantly longer in comparison with the referent compound (1-pyrenebutyric acid: 2.5 and 100.3 ns) (Table S1†). In addition, the relative quantum yields of **1**/BSA and **2**/BSA (Φ_f < 0.01) were much lower in comparison with those of referent 1-pyrenebutyric acid (Φ_f < 0.15 ± 0.02). Such differences are due to the microenvironment of the pyrene chromophore; that is, referent 1-pyrenebutyric acid is completely solvated in water, whereas pyrenes from **1** and **2** are deeply inserted into the BSA binding site and efficiently shielded from the aqueous environment but distanced from Ru/aryl interactions, which quenched pyrene emission in water. Multivariate analysis of titration data using the Specfit program[54,55] gave the best fit for 1 : 1 complex formation, with a binding constant of log K_s = 5.15 ± 0.06 (**1**) or log K_s = 5.23 ± 0.07 (**2**), as reported previously for similar compounds.[42]

A comparison of degassed and non-degassed samples shows a minor effect of oxygen on fluorescence, indicating that the fluorophore is shielded from the solvent in the BSA complex and ligand **L**, indicating a change in the electronic properties of the studied compounds (Table S1†).

Cytotoxicity

The MTT[56] assay on a human cervical carcinoma (HeLa) cell line, widely accepted for testing new compounds[57] (Table S2†), revealed ruthenium pyrene complexes interesting for further examination as potential antitumor compounds. The mono-pyrene analogue **1** (IC_{50} 5.13 ± 1.10 μM) has been shown to be more cytotoxic than bis-pyrene **2** (IC_{50} 12.50 ± 0.50 μM). The toxicity of ruthenium phosphine-based complexes was reported previously on different types of tumour cancer cell lines.[42] Only mono-pyrene **1** showed an order of magnitude lower activity towards a normal human cell line (Table S2†), thus being selective against tumour cells. We previously reported the selectivity of ruthenium phosphine-based complexes toward normal human cell lines, fibroblasts and keratinocytes, compared with different types of cancer cells.[42] Additionally, this feature was determined for ruthenium arene complexes with triphenylphosphine ligands tested on pancreatic cancer cells compared with the mouse embryo fibroblast Balb/3T3 clone A31 cell line.[58]

Upon UV light irradiation, both compounds **1** and **2** exhibited an increased effect on cell viability (Fig. 5) with IC_{50} values of 3.24 ± 0.4 μM and 8.75 ± 1.8 μM, respectively, which is attributed to singlet oxygen activation by pyrene. It is interesting that despite the abovementioned toxicity of similar compounds, the one described here displays more potential upon stimulation by UV irradiation. This suggests a need to consider them in the context of the possible TPA agents.

Conclusion

In conclusion, we have prepared two ruthenium complexes characterised by complete fluorescence quenching of pyrene, as a consequence of pyrene interaction with aryl-substituents and ruthenium cations. The binding of **1** or **2** to BSA regained the emission; thus **1** or **2** acts as a fluorescent beacon-sensor for BSA, while being non-active against *ds*-DNA. Moreover, both compounds exhibit cytotoxicity, whereby only the mono-pyrene analogue is selective against tumour (HeLa) cells in comparison with normal cells. The bioactivity is enhanced by UV irradiation, supporting further development of photodynamic TPA probes.[31–34]

Experimental section

General methods

Chemicals were used as purchased from commercial suppliers without further purification. Reactions were carried out in ordinary glassware and were monitored by TLC on silica gel 60 F_{254} plates and detected with a UV lamp (254 nm). Purification of crude products was performed using an automated flash chromatography system, equipped with a UV detector (254 nm) and prepacked silica columns (silica, RediSep), or by manual column chromatography. NMR spectra were obtained on spectrometers operating at 300.13 or 600.13 MHz for ^{1}H,

75.47 or 150.92 MHz for ^{13}C and 242.93 MHz for ^{31}P nuclei. Chemical shifts, δ/ppm, indicate a downfield shift from the internal standard tetramethylsilane (TMS) for the ^{1}H NMR or residual solvent signal for ^{13}C NMR (77.16 ppm for $CDCl_3$) and H_3PO_4 (85%) for ^{31}P NMR. Coupling constants, J, are given in Hz. High-resolution mass spectra were obtained on a MALDI TOF-TOF instrument using a CHCA matrix. UV-vis spectra were recorded on a Varian Cary 50 spectrophotometer and CD spectra were recorded on a JASCO J-810 spectropolarimeter equipped with a Peltier thermostat in 0.1 cm or 1 cm quartz Suprasil cells. Infrared spectra were measured with a Bruker Alpha-T FT-IR spectrometer in the solid state (KBr pastille) and in solution (KBr cuvette, DCM). Fluorescence spectra were recorded on a Varian Cary Eclipse fluorimeter.

Peptide coupling

An acid (1 eq.), TBTU (1 eq.), HOBt (1 eq.) and DIPEA (2 eq.) were added to CH_2Cl_2 and stirred at room temperature (r.t.) for 1 hour. After activation, a mono-substituted diamine was added (1 eq.) and the reaction mixture was stirred at r.t. for 2 days. The reaction mixture was washed with saturated $NaHCO_3$, 10% citric acid and water, and then dried over anhydrous Na_2SO_4. The reaction mixture was then evaporated onto silica gel and purified by automated flash chromatography on a prepacked silica column (12 g) with an EtOAc/hexane gradient.

Boc-protecting group removal

Boc protected compounds (**P**) were dissolved in 10 ml DCM/trifluoroacetic acid (1/1) and stirred for 2 hours at room temperature. The volatiles were evaporated under reduced pressure and the residue was dissolved in 15 ml of CH_2Cl_2. The remaining trifluoracetic acid was neutralized with an excess of DIPEA (1 ml). This solution was used for further coupling reactions.

Compound characterization

P: 1-Pyrenebutyric acid (250 mg, 0.87 mmol), *N*-boc-ethylenediamine (140 μL, 0.87 mmol), HOBt (118 mg, 0.87 mg), TBTU (279 mg, 0.87 mg), DIPEA (590 μl, 3.48 mmol), and DCM (100 ml). Chromatography: silica (12 g flash column), EtOAc/hexane gradient (50–70% EtOAc). Yield: 243 mg (65%) of precursor **P**. ^{1}H NMR (300 MHz, $CDCl_3$) δ = 8.30 (d, J = 9.3, 1H), 8.14 (dd, J = 16.3, 8.7, 4H), 8.06–7.94 (m, 3H), 7.86 (d, J = 7.8, 1H), 6.11 (s, 1H), 4.88 (s, 1H), 3.44–3.31 (m, 4H), 3.27 (s, 2H), 2.37–2.14 (m, 4H), 1.37 (s, 9H).

L: Precursor **P** (240 mg, 0.56 mmol), 3-(diphenylphosphino)-benzoic acid (172 mg, 0.56 mmol), HOBt (76 mg, 0.56 mg), TBTU (180 mg, 0.56 mg), DIPEA (380 μl, 2.24 mmol), DCM (100 ml). Chromatography: silica (12 g flash column), EtOAc/hexane gradient. Yield: 289 mg (83%) of ligand **L**. ^{1}H NMR (300 MHz, $CDCl_3$) δ = 8.24 (d, J = 9.3, 1H), 8.15 (dd, J = 7.6, 2.3, 2H), 8.06 (d, J = 8.5, 2H), 8.02–7.94 (m, 3H), 7.85–7.76 (m, 2H), 7.75–7.68 (m, 1H), 7.33–7.24 (m, 12H). ^{13}C NMR (151 MHz, $CDCl_3$) δ = 174.50 (s), 168.12 (s), 138.63 (d, J = 13.5), 136.69 (s), 136.68 (s), 136.61 (s), 136.59 (s), 135.80 (s), 134.29 (s), 134.24 (s), 133.89 (d, J = 19.7), 132.53 (d, J = 24.8), 131.54 (s), 131.01 (s), 130.08 (s), 129.07 (s), 128.93 (d, J = 5.4), 128.87 (s, J = 5.0), 128.75 (d, J = 7.1), 127.58 (d, J = 11.3), 127.42 (d, J = 10.3), 126.86 (s), 126.00 (s), 125.16 (d, J = 15.7), 125.07 (s), 124.94 (s), 123.44 (s), 41.42 (s), 40.02 (s), 36.02 (s), 32.80 (s), 27.42 (s). ^{31}P NMR (243 MHz, $CDCl_3$) δ = −5.27 (d, J = 41.4). MALDI-HRMS (m/z): calculated: 619.2514 ($C_{41}H_{35}N_2O_2P^+$, $[M + H]^+$); found: 619.2512.

1: Ligand **L** (124 mg, 0.2 mmol) was dissolved in DCM (5 mL), di-μ-chlorobis[(*p*-cymene)chlororuthenium(II)] (61 mg, 0.1 mmol) was added and stirred for 2 h. After the reaction, the crude product was purified by column chromatography on a short silica column (20 g), using an DCM/MeOH eluent (2–3% MeOH). Yield: 166 mg (90%) of mono-complex **1**. ^{1}H NMR (300 MHz, $CDCl_3$) δ = 9.04 (d, J = 12.8, 1H), 8.41 (d, J = 9.3, 1H), 8.20–8.10 (m, 4H), 8.06–7.93 (m, 5H), 7.87–7.72 (m, 5H), 7.53–7.39 (m, 6H), 6.99 (s, 2H), 4.90 (s, 4H), 3.64–3.43 (m, 6H), 2.65–2.50 (m, 3H), 2.38–2.26 (m, 2H), 1.77 (s, 3H), 0.89 (d, J = 6.9, 6H). ^{13}C NMR (151 MHz, $CDCl_3$) δ = 173.68 (s), 167.97 (s), 136.91 (s), 136.79 (s), 136.67 (s), 135.08 (s), 134.45 (s), 134.15 (s), 133.72 (s), 133.66 (s), 133.55 (s), 133.47 (s), 131.55 (s), 131.12 (s), 131.09 (s), 130.98 (d, J = 2.1), 130.78 (s), 129.95 (s), 129.68 (d, J = 2.2), 128.96 (s), 128.67 (s), 128.60 (s), 128.37 (s), 128.32 (s), 127.67 (s), 127.57 (s), 127.49 (s), 126.69 (s), 125.90 (s), 125.19 (d, J = 7.5), 125.03 (s), 124.87 (d, J = 2.7), 123.83 (s), 110.34 (s), 95.47 (s), 90.23 (s), 90.20 (s), 86.27 (s), 86.23 (s), 40.15 (s), 40.06 (s), 36.16 (s), 33.10 (s), 30.37 (s), 27.58 (s), 21.70 (s), 17.50 (s). ^{31}P NMR (243 MHz, $CDCl_3$) δ = 23.08 (s). MALDI-HRMS (m/z): calculated: 924.1952 ($C_{51}H_{49}Cl_2N_2O_2P^+$, $[M]^+$); found: 924.1950.

2: Mono-complex **1** (60 mg, 0.065 mmol) and NH_4PF_6 (16 mg, 0.098 mmol) were dissolved in CH_3CN (7 mL) and refluxed for 35–45 min. CH_3CN was evaporated and the residue was dissolved in DCM (5 mL). Ligand **L** (101 mg, 0.16 mg) was added and the mixture was stirred for 24 h. The crude product was purified by column chromatography on silica (35 g), using an DCM/MeOH eluent (2–5% MeOH). Yield: 26 mg (24%) of bis-complex **2**. ^{1}H NMR (300 MHz, $CDCl_3$) δ = 8.21 (d, J = 9.2, 2H), 8.08–8.03 (m, 4H), 7.99–7.92 (m, 6H), 7.90–7.86 (m, 5H), 7.83–7.72 (m, 8H), 7.37 (d, J = 7.1, 5H), 7.21–6.96 (m, 16H), 6.71 (s, 2H), 5.02 (d, J = 6.6, 2H), 4.87 (s, 2H), 3.52 (s, 10H), 3.29–3.21 (m, 4H), 2.42–2.28 (m, 5H), 2.16–2.03 (m, 5H), 1.13 (d, J = 7.0, 6H).^{13}C NMR (151 MHz, $CDCl_3$) δ = 174.83 (s), 166.63 (s), 136.36 (s), 136.34 (d, J = 7.2), 134.36 (t, J = 4.7), 133.82 (t, J = 3.9), 132.76 (s), 131.50 (s), 131.42 (s), 130.98 (s), 130.71 (s), 129.85 (s), 129.47 (s), 128.88–128.78 (m), 128.77 (s), 128.72–128.57 (m), 128.51–128.35 (m), 127.59 (s), 127.54 (s), 127.46 (s), 126.65 (s), 125.91 (s), 125.01 (s), 124.99 (s), 124.94 (s), 124.86 (d, J = 3.1), 123.66 (s), 99.52 (s), 97.16 (s), 88.63 (s), 41.34 (s), 39.60 (s), 36.33 (s), 33.09 (s), 31.17 (s), 28.07 (s), 21.37 (s), 14.41 (s). ^{31}P NMR (243 MHz, $CDCl_3$) δ = 20.97 (s), −135.20 – −152.85 (m). MALDI-HRMS (m/z): calculated: 1473.50841 ($C_{74}H_{77}N_4O_4P_2Ru^+$, $[M - PF_6 - Cl + H^-]^+$), found: 1473.5270.

MTT test procedure

Cells were seeded into 96-well tissue culture plates and the next day different concentrations of **1** or **2** were added to each

well in quadruplicate. An hour and a half later, cells were either irradiated using UV light (350 nm, 90 s) or not. Following 72 h of incubation at 37 °C, the medium was aspirated, and the MTT dye was added. Three hours later, the formazan crystals formed were dissolved in DMSO, the plates were mechanically agitated for 5 min and the optical density at 545 nm was determined on a microtiter plate reader. The percent of life cells was calculated as follows: % = OD (sample) − OD (background)/OD (control) − OD (background) × 100. The optical density (OD) of the background for adherent cells is the OD of the MTT solution and DMSO; the OD (background) for suspension cells is the OD of the culture medium with MTT and 10% SDS with 0.01 mol L^{-1} HCl; OD (control) is the OD of the cell growth without the tested compounds. The results were expressed as IC_{50}, a concentration of the compound which decreases the cell viability to 50% compared to non-treated control cell viability set to 100%.

Conflicts of interest

There are no conflicts to declare.

Acknowledgements

This work was supported by CAT Pharma (KK.01.1.1.04.0013), a project co-financed by the Croatian Government and the European Union through the European Regional Development Fund – the Competitiveness and Cohesion Operational Programme and the CSF project IP-2018-01-5475 and DOK-2018-01-8086. We thank MSc. Marta Jurković for help with TR-FL spectroscopy.

References

1 A. Jahanban-Esfahlan, A. Ostadrahimi, R. Jahanban-Esfahlan, L. Roufegarinejad, M. Tabibiazar and R. Amarowicz, *Int. J. Biol. Macromol.*, 2019, **138**, 602–617.
2 Z. He, C. Ke and B. Z. Tang, *ACS Omega*, 2018, **3**, 3267–3277.
3 M. M. Islam, Z. Hu, Q. Wang, C. Redshaw and X. Feng, *Mater. Chem. Front.*, 2019, **3**, 762–781.
4 K. Y. Pu and B. Liu, *J. Phys. Chem. B*, 2010, **114**, 3077–3084.
5 C. M. Moore, D. Pendse and M. Emberton, *Nat. Clin. Pract. Urol.*, 2009, **6**, 18–30.
6 W. Fan, P. Huang and X. Chen, *Chem. Soc. Rev.*, 2016, **45**, 6488–6519.
7 K. Yamana, H. Zako, K. Asazuma, R. Iwase, H. Nakano and A. Murakami, *Angew. Chem., Int. Ed.*, 2001, **40**, 1104–1106.
8 V. A. Korshun, D. A. Stetsenko and M. J. Gait, *J. Chem. Soc., Perkin Trans. 1*, 2002, 1092–1104.
9 L. Hernandez-Folgado, D. Baretić, I. Piantanida, M. Marjanović, M. Kralj, T. Rehm and C. Schmuck, *Chem. – Eur. J.*, 2010, **16**, 3036–3056.
10 J. Wu, Y. Zou, C. Li, W. Sicking, I. Piantanida, T. Yi and C. Schmuck, *J. Am. Chem. Soc.*, 2012, **134**, 1958–1961.
11 F. Ma, W. Liu, Q. Zhang and C. Zhang, *Chem. Commun.*, 2017, **53**, 10596–10599.
12 E. Kostenko, M. Dobrikov, D. Pyshnyi, V. Petyuk, N. Komarova, V. Vlassov and M. Zenkova, *Nucleic Acids Res.*, 2001, **29**, 3611–3620.
13 A. Mahara, R. Iwase, T. Sakamoto, K. Yamana, T. Yamaoka and A. Murakami, *Angew. Chem., Int. Ed.*, 2002, **41**, 3648–3650.
14 I. V. Astakhova, D. Lindegaard, V. A. Korshun and J. Wengel, *Chem. Commun.*, 2010, **46**, 8362–8364.
15 U. B. Christensen and E. B. Pedersen, *Nucleic Acids Res.*, 2002, **30**, 4918–4925.
16 V. V. Filichev and E. B. Pedersen, *Org. Biomol. Chem.*, 2003, **1**, 100–103.
17 K. Gröger, D. Baretić, I. Piantanida, M. Marjanović, M. Kralj, M. Grabar, S. Tomić and C. Schmuck, *Org. Biomol. Chem.*, 2011, **9**, 198–209.
18 I. V. Astakhova, A. D. Malakhov, I. A. Stepanova, A. V. Ustinov, S. L. Bondarev, A. S. Paramonov and V. A. Korshun, *Bioconjugate Chem.*, 2007, **18**, 1972–1980.
19 L. Hernandez-Folgado, C. Schmuck, S. Tomić and I. Piantanida, *Bioorg. Med. Chem. Lett.*, 2008, **18**, 2977–2981.
20 Ž. Ban, J. Matić, B. Žinić, A. Foller Füchtbauer, L. M. Wilhelmsson and I. Piantanida, *Molecules*, 2020, **25**, 2188.
21 N. Vân Anh, F. Schlosser, M. M. Groeneveld, I. H. M. van Stokkum, F. Würthner and R. M. Williams, *J. Phys. Chem. C*, 2009, **113**, 18358–18368.
22 N. Basilio, L. Garcia-Rio and M. Martin-Pastor, *J. Phys. Chem. B*, 2010, **114**, 4816–4820.
23 K. L. Chan, J. P. F. Lim, X. Yang, A. Dodabalapur, G. E. Jabbour and A. Sellinger, *Chem. Commun.*, 2012, **48**, 5106–5108.
24 E. A. Vasilieva, G. A. Gainanova, A. M. Bekmukhametova, T. R. Karimova, M. N. Saifutdinova, E. L. Gavrilova, L. Y. Zakharova and O. G. Sinyashin, *Russ. Chem. Bull.*, 2015, **64**, 2897–2902.
25 V. Burilov, R. Garipova, E. Sultanova, D. Mironova, I. Grigoryev, S. Solovieva and I. Antipin, *Nanomaterials*, 2020, **10**, 1143.
26 L. Guerrini, J. V. Garcia-Ramos, C. Domingo and S. Sanchez-Cortes, *Anal. Chem.*, 2009, **81**, 953–960.
27 S. K. Dinda, M. Althaf Hussain, A. Upadhyay and C. P. Rao, *ACS Omega*, 2019, **4**, 17060–17071.
28 P. Leyton, S. Sanchez-Cortes, J. V. Garcia-Ramos, C. Domingo, M. Campos-Vallette, C. Saitz and R. E. Clavijo, *J. Phys. Chem. B*, 2004, **108**, 17484–17490.
29 N. Pragti, B. K. Kundu, S. N. Upadhyay, N. Sinha, R. Ganguly, I. Grabchev, S. Pakhira and S. Mukhopadhyay, *Dalton Trans.*, 2022, **51**, 3937–3953.
30 B. K. Banik and F. F. Becker, *Curr. Med. Chem.*, 2001, **8**, 1513–1533.
31 T. Kanamori, A. Matsuyama, H. Naito, Y. Tsuga, Y. Ozako, S. Ogura, S. Okazaki and H. Yuasa, *J. Org. Chem.*, 2018, **83**, 13765–13775.

32 W. Wu, X. Shao, J. Zhao and M. Wu, *Adv. Sci.*, 2017, **4**, 1700113.
33 F. Bolze, S. Jenni, A. Sour and V. Heitz, *Chem. Commun.*, 2017, **53**, 12857–12877.
34 M. Rumi and J. W. Perry, *Adv. Opt. Photonics*, 2010, **2**, 451–518.
35 B. Sun, L. Wang, Q. Li, P. He, H. Liu, H. Wang, Y. Yang and J. Li, *Biomacromolecules*, 2017, **18**, 3506–3513.
36 Y. Yang, L. Wang, H. Cao, Q. Li, Y. Li, M. Han, H. Wang and J. Li, *Nano Lett.*, 2019, **19**, 1821–1826.
37 S. Thota, D. A. Rodrigues, D. C. Crans and E. J. Barreiro, *J. Med. Chem.*, 2018, **61**, 5805–5821.
38 X. Hu, L. Guo, M. Liu, Q. Zhang, Y. Gong, M. Sun, S. Feng, Y. Xu, Y. Liu and Z. Liu, *Inorg. Chem.*, 2022, **61**, 20008–20025.
39 C. Sonkar, S. Sarkar and S. Mukhopadhyay, *RSC Med. Chem.*, 2022, **13**, 22–38.
40 S. Swaminathan, J. Haribabu, N. Balakrishnan, P. Vasanthakumar and R. Karvembu, *Coord. Chem. Rev.*, 2022, **459**, 214403.
41 T. R. Steel, F. Walsh, A. Wieczorek-Błauż, M. Hanif and C. G. Hartinger, *Coord. Chem. Rev.*, 2021, **439**, 213890.
42 M. Pernar, Z. Kokan, J. Kralj, Z. Glasovac, L. M. Tumir, I. Piantanida, D. Eljuga, I. Turel, A. Brozovic and S. I. Kirin, *Bioorg. Chem.*, 2019, **87**, 432–446.
43 S. Opačak, Z. Kokan, Z. Glasovac, B. Perić and S. I. Kirin, *Eur. J. Org. Chem.*, 2019, 2115–2128.
44 S. Opačak, D. Babić, B. Perić, Ž. Marinić, V. Smrečki, B. Pem, I. Vinković Vrček and S. I. Kirin, *Dalton Trans.*, 2021, **50**, 4504–4511.
45 Y. B. Chen, K. Li, S. S. Zhang, P. Xu and B. Song, *Dyes Pigm.*, 2022, **202**, 110267.
46 Y. D. Hang, L. Yang, Y. Qu and J. L. Hua, *Tetrahedron Lett.*, 2014, **55**, 6998–7001.
47 E. Babu, P. Muthu Mareeswaran, S. Singaravadivel, J. Bhuvaneswari and S. Rajagopal, *Spectrochim. Acta, Part A*, 2014, **130**, 553–560.
48 R. K. Vuradi, S. Avudoddi, V. R. Putta, L. R. Kotha, P. K. Yata and S. Sirasani, *J. Fluoresc.*, 2017, **27**, 939–952.
49 R. K. Vuradi, V. R. Putta, D. Nancherla and S. Sirasani, *J. Fluoresc.*, 2016, **26**, 689–701.
50 R. J. Lakowicz, *Principles of Fluorescence Spectroscopy*, Springer, New York, 3rd edn, 2006.
51 I. Orehovec, D. Glavač, I. Dokli, M. Gredičak and I. Piantanida, *Croat. Chem. Acta*, 2017, **90**, 603–611.
52 J. Matić, T. Tandarić, M. R. Stojković, F. Šupljika, R. Vianello and L.-M. Tumir, *Beilstein Arch.*, 2023, **2023**, 1.
53 A. C. Sedgwick, J. T. Brewster, T. Wu, X. Feng, S. D. Bull, X. Qian, J. L. Sessler, T. D. James, E. V. Anslyn and X. Sun, *Chem. Soc. Rev.*, 2021, **50**, 9–38.
54 H. Gampp, M. Maeder, C. J. Meyer and A. D. Zuberbühler, *Talanta*, 1985, **32**, 257–264.
55 M. Maeder and A. D. Zuberbuehler, *Anal. Chem.*, 1990, **62**, 2220–2224.
56 J. van Meerloo, G. J. L. Kaspers and J. Cloos, *Methods Mol. Biol.*, 2011, **731**, 237–245.
57 P. Mirabelli, L. Coppola and M. Salvatore, *Cancers*, 2019, **11**(8), 1098.
58 L. Biancalana, A. Pratesi, F. Chiellini, S. Zacchini, T. Funaioli, C. Gabbiani and F. Marchetti, *New J. Chem.*, 2017, **41**, 14574–14588.
59 I. Krošl, M. Košćak, K. Ribičić, B. Žinić, D. Majhen, K. Božinović and I. Piantanida, *Int. J. Mol. Sci.*, 2022, **23**, 7006.